Volume 10, Number 2, 2024

High-Fidelity RANS CFD Simulations of Physico-Chemical Process of Combustion in Gas Turbine Combustion Chambers in ANSYS CFX

Masoud Hajivand*

National Aerospace University "Kharkiv Aviation Institute", 17 Vadym Manko St., Kharkiv, 61070, Ukraine

Received: October 02, 2024. Revised: October 30, 2024. Accepted: November 06, 2024.

Abstract

This study examines the validation and precision of essential parameters, including temperature distribution and nitrogen oxide (NO_x) emissions, at the outlet of a gas turbine combustion chamber through high-fidelity Reynolds-Averaged Navier-Stokes (RANS) CFD simulations. The propane(C_3H_8)-air combustion process is modeled in ANSYS CFX utilizing three various turbulence models, including standard k-ε, RNG k-ε, and shear stress transport (SST), beside various combustion models such as the Eddy Dissipation Model (EDM), a hybrid of Eddy Dissipation and Finite Rate Chemistry (EDM/FRC), and the Flamelet model, including the P-1 model of radiation. A thorough sensitivity analysis was performed utilizing fine, medium, and coarse unstructured computational meshes to improve the reliability and accuracy of the results. The obtained CFD results showed that for outlet temperature, the standard k-ε turbulence model coupled with the Flamelet combustion model yields a mean deviation of -6.8%, while k-ε coupled with EDM yields a mean deviation of -9.9%. It also gave the lowest deviation of NO_x emissions at combustor outlet equal to 2.3% when EDM/FRC combustion model was used in tandem with SST turbulence model. While the same combustion model coupled with the standard k-ε and RNG k-ε turbulence models exhibited a higher mean deviation of 13.6% and 15.4%, respectively, in predicting NO_x emissions.

Keywords: combustion; emission; CFD; turbulence; Flamelet model; validation; eddy dissipation.

1. Introduction

For computational fluid dynamics (CFD) models used in physico-chemical processes in combustion chambers to be accurate and reliable, verification and validation, or V&V, is crucial. Confirming that the model is applied successfully and that the equations are solved as expected are the main goals of verification. This entails determining whether the CFD program is accurate, evaluating numerical errors, doing time-step sensitivity assessments and grid convergence, and comparing the findings with analytical solutions or benchmark examples in order to weed out mistakes and verify the solution of model equations.

However, validation makes sure that the model correctly captures occurrences that occur in the real world. The process entails acquiring superior experimental data or field measurements to function as benchmarks, fine-tuning the model to more closely align with this information, and contrasting significant simulation outcomes like temperature profiles, pressure distributions, velocity fields, and species concentrations with experimental data, particularly in the combustor exit. The degree of agreement between simulation and experimental results is measured using statistical techniques, and the robustness of the model is evaluated and significant parameters are identified through sensitivity analysis. To determine the level of confidence in model predictions, uncertainty quantification takes measurement errors, model assumptions, and numerical uncertainties into account. To prove that the CFD model is credible, the entire validation process, including experimental setup, data collection, calibration, comparison results, and

* Corresponding author. Email address: m.hajivand82@gmail.com

This paper should be cited as: M. Hajivand. High-fidelity RANS CFD simulations of physico-chemical process of combustion in gas turbine combustion chambers in ANSYS CFX. *Energy Engineering and Control Systems*, 2024, Vol. 10, No. 2, pp. 81 – 95. https://doi.org/10.23939/jeecs2024.02.081

uncertainties should be carefully recorded. Verification deals with the relationship between the conceptual model and the computerized model, whereas validation deals with the relationship between the computerized model and reality (see Fig.1). In alternative formulations of V&V, these linkages are not usually acknowledged [1],[2].

As shown in Fig.2, these two procedures serve as foundational steps for the generation of a precise and trustworthy numerical solution. Verification must precede validation, and in turn, validation has to be in place before arriving at intended numerical results [3].

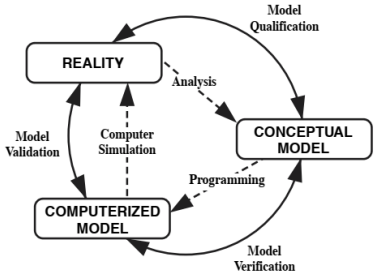

Fig.1. Phases of modeling and simulation and the role of V&V [2].

The purpose of verification is to guarantee that the computational model is applied accurately and flawlessly. It must be confirmed that the CFD code correctly solves the equation of state, the fundamental equations of fluid dynamics, and any potential turbulence models. The developer of the CFD program will very certainly have already verified this entire numerical model. This check makes sure the code functions properly. To ensure that the model accurately captures physical reality, the numerical outputs are cross-checked against experimental or other real-world data throughout the validation phase. Developing confidence that the numerical answers are both physically meaningful and mathematically valid requires completion of this step.

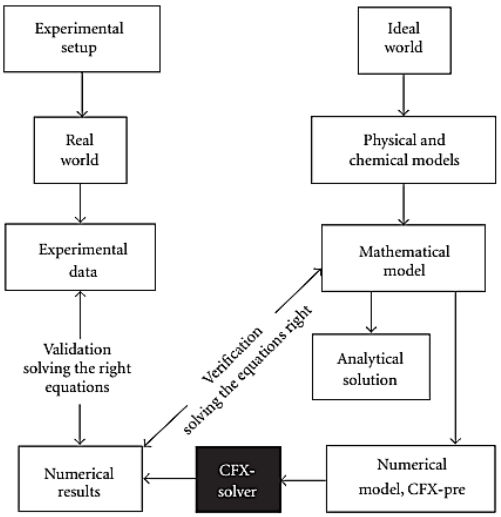

Fig.2. Logic scheme of validation and verification implementing by ANSYS CFX [3].

Software users must validate their user-defined specialized models, even if the creators of the CFD algorithms are often responsible for verifying the fundamental elements. Custom boundary conditions, distinct fluid characteristics, or study-specific geometries could be the cause. In order to obtain reliable and valid results, a user must carefully verify and validate the accuracy and dependability of CFD simulations. All of these actions are necessary to maintain integrity in computational research so that accurate and trustworthy simulations can advance the science of fluid dynamics [3].

Validation and verification of Computational Fluid Dynamics (CFD) models for combustion processes in combustion chambers have been subjects of extensive research due to their complexity and importance in various applications, including power generation, propulsion systems, and industrial furnaces.

2. Analysis of the recent publications and research works

Using the combination of CFD models and experimental research, Bhurat, S. et al. [4] verified their findings. Evaluation of the combustion, performance, and emission characteristics of a modified single-cylinder engine running in the partially pre-mixed charge compression ignition (PCCI) mode was the focus of the experimental setup. At various engine loads, they measured variables such brake thermal efficiency, exhaust gas temperature, volumetric efficiency, pressure, net heat release rate, and emissions. In order to examine the turbulence and velocity change of the air-fuel mixture in the redesigned intake manifold, the authors also carried out CFD tests. The ANSYS fluid flow (CFX) software was used to run these CFD simulations in order to evaluate how the changed intake manifold affected the parameters of the air-fuel mixture.

Stereoscopic particle image velocimetry (SPIV) was employed by Becker, L. et al. [5] to measure the combustor's flow field. To locate the reaction zone, they also used planar laser-induced fluorescence of the hydroxyl radical (OH-PLIF). These experimental observations were made downstream of the drop plane and inside the quart to confirm the outcomes of the large-eddy models. To confirm their conclusions, the authors also contrasted the outcomes of non-reactive flow conditions with the matching reactive operating conditions.

Assad Masri, professor at the University of Sydney, contributed to combustion science through experimental work that has contributed quite substantially toward validating most combustion CFD models. His research focuses on quantitative provision of high-quality experimental data about phenomena in turbulent combustion. Among Masri's major contributions is the development of the Sydney Swirl Burners [6]. This experimental setup allows studies on swirling flames to be organized in essentially all different conditions. The burner has created large resultant datasets, considerably used in validation procedures involving computational models right from RANS to LES and PDF methods.

In the subject of combustion, there is now healthy competition between experimental and numerical scientists thanks to the development of computational approaches [7] and sophisticated experimental diagnostic techniques [8],[9]. CFD was developed in the second part of the 20th century to provide numerical solutions for the Reynolds averaged Navier-Stokes (RANS) equations [10]. Thanks to this development, scientists were able to reproduce the basic statistical features of turbulent flames, such as mean and root mean square (RMS) variations in temperature, density, velocity, and even composition fields [11]. However, it took several years before experimental techniques could produce the necessary data to validate these computational models [10].

In addition to verifying previous computational predictions, the use of these sophisticated diagnostic techniques in experimental combustion research has revealed unexpected phenomena that both challenge and improve upon existing numerical models. Our understanding of combustion processes has significantly improved as a result of the iterative process of creating and testing CFD models using state-of-the-art experimental data [10]. It has also highlighted how crucial it is for computational and experimental scientists to work together to advance our understanding of turbulent combustion. This complementary relationship keeps pushing advances in experimental and numerical methodologies, resulting in increasingly precise and thorough models of combustion events [10].

3. The main goal of this investigation

The purpose of this research is to analyze how various models of turbulence and combustion, perform and behave in the process of propane-air combustion in a gas turbine combustion chamber accurately and effectively using ANSYS CFX software. The main purpose is to evaluate performance critical parameters like temperature distribution and nitrogen oxide (NO_x) emissions at the outlet of the combustion chamber. Additionally, the investigation explores how mesh resolution impacts simulation accuracy through sensitivity analysis, concentrating on the combination of turbulence and combustion models in the related software. The results aim to help enhance the accuracy of the results obtained in CFD combustion simulation, leading to better gas turbine combustor designs that exhibit performance and lower emissions at the outlet.

4. Governing equations

The multi-component, turbulent, chemically reacting system's differential equations for mass, impulse, and energy conservation must be solved in order to model the physical and chemical processes occurring in the

combustion chamber of a gas turbine [13]. A mass conservation equation or the continuity equation for compressible and incompressible media can be represented as follows [13],[14]:

$$\frac{\partial \rho}{\partial t} + \nabla(\rho \vec{v}) = S_m, \tag{1}$$

where ρ is mass density of flow; $\vec{v}$ is a local flow velocity vector; S_m is a source term which defines the mass supplied to the flow.

The momentum conservation equation in a fixed system of reference may be formed as [13]-[15]:

$$\frac{\partial}{\partial t}(\rho \vec{\mathrm{v}}) + \nabla(\rho \vec{u} \vec{v}) = -\nabla p + \nabla \cdot (\tau_{st}) + \rho \vec{\mathrm{g}} + \vec{F}, \tag{2}$$

where p is the static pressure; τ_{st} is the stress tensor; $\rho \vec{\mathrm{g}}$ and $\vec{F}$ are the gravitational body force and external body forces, respectively.

In a generalised form, the energy conservation equation can be written as:

$$\frac{\partial}{\partial t}(\rho E) + \nabla \cdot (\vec{\mathrm{v}}(\rho E + p)) = \nabla \cdot \left(k_{eff} \nabla T - \sum_j \vec{J}_j + \left(\bar{\bar{\tau}}_{eff} \cdot \vec{\mathrm{v}} \right) \right) + S_h, \tag{3}$$

where E is the total energy; k_{eff} is the effective conductivity; $\vec{J}_j$ is the diffusion flux of species j; $\bar{\bar{\tau}}_{eff}$ is the effective viscosity coefficient; S_h is the heat of the chemical reaction.

5. Mathematical description of k-ε turbulent model in ANSYS CFX

Since two-equation turbulence models provide a good balance between computational accuracy and numerical effort, they are widely used [12]. Compared to zero equation models, two-equation models are substantially more complex. The term "two-equation" refers to the fact that the velocity and length scale are solved using different transport equations.The gradient diffusion hypothesis is used by the k-ε model to establish a relationship between the turbulent viscosity and mean velocity gradients and Reynolds stresses. In this model, the turbulent kinetic energy, which comes from solving its transport equation, is used to calculate the turbulence velocity scale. Usually, the turbulent kinetic energy and its dissipation rate are the two properties of the turbulence field that are used to estimate the turbulent length scale. The solution to its transport equation yields the turbulent kinetic energy dissipation rate [12].

In k-ε model, k is the turbulence kinetic energy and is defined as the variance of the fluctuations in velocity. It has dimensions of (L^2T^{-2}), for example, $\mathrm{m}^2/\mathrm{s}^2$. ε is the turbulence eddy dissipation (the rate at which the velocity fluctuations dissipate), and has dimensions of per unit time (L^2T^{-3}), for example, $\mathrm{m}^2/\mathrm{s}^3$ [12].

The k-ε model introduces two new variables into the system of equations. The continuity equation is then

$$\frac{\partial \rho}{\partial t} + \frac{\partial}{\partial x_j}(\rho U_j) = 0, \tag{4}$$

and the momentum equation becomes

$$\frac{\partial \rho U_i}{\partial t} + \frac{\partial}{\partial x_j}(\rho U_i U_j) = -\frac{\partial p'}{\partial x_i} + \frac{\partial}{\partial x_j}\left[\mu_{eff} \left(\frac{\partial U_i}{\partial x_j} + \frac{\partial U_j}{\partial x_i} \right) \right] + S_M, \tag{5}$$

where S_M is the sum of body forces; μ_{eff} is the effective viscosity accounting for turbulence; p' is the modified pressure as defined in equation (6) [12].

$$p' = p + \frac{2}{3}\rho k + \frac{2}{3}\mu_{eff} \frac{\partial U_k}{\partial x_k}. \tag{6}$$

The k-ε model, is based on the eddy viscosity concept, so that:

$$\mu_{\mathrm{eff}} = \mu + \mu_t, \tag{7}$$

where μ_t is the turbulence viscosity.

The k-ε model assumes that the turbulence viscosity is linked to the turbulence kinetic energy and dissipation via the relation where C_μ is a constant [12]:

$$\mu_t = C_\mu \rho \frac{k^2}{\varepsilon}. \tag{8}$$

The values of k and ε come directly from the differential transport equations for the turbulence kinetic energy and turbulence dissipation rate [12]:

$$\frac{\partial(\rho k)}{\partial t} + \frac{\partial}{\partial x_j}(\rho U_j k) = \frac{\partial}{\partial x_j}\left[\left(\mu + \frac{\mu_t}{\sigma_k}\right)\frac{\partial k}{\partial x_j}\right] + P_k - \rho\varepsilon + P_{kb}, \tag{9}$$

$$\frac{\partial(\rho \varepsilon)}{\partial t} + \frac{\partial}{\partial x_j}(\rho U_j \varepsilon) = \frac{\partial}{\partial x_j}\left[\left(\mu + \frac{\mu_t}{\sigma_\varepsilon}\right)\frac{\partial \varepsilon}{\partial x_j}\right] + \frac{\varepsilon}{k}(C_{\varepsilon 1} P_k - C_{\varepsilon\varepsilon}\rho\varepsilon + C_{\varepsilon 1} P_{\varepsilon b}), \tag{10}$$

where $C_{\varepsilon 1}, C_{\varepsilon 2}, \sigma_k$ and σ_ε, are constants [12].

P_{kb} and $P_{\varepsilon b}$ represent the influence of the buoyancy forces, which are described below. P_k is the turbulence production due to viscous forces, which is modeled using:

$$P_k = \mu_t\left(\frac{\partial U_i}{\partial x_j} + \frac{\partial U_j}{\partial x_i}\right)\frac{\partial U_i}{\partial x_j} - \frac{2}{3}\frac{\partial U_k}{\partial x_k}\left(3\mu\frac{\partial U_k}{\partial x_k} + \rho k\right). \tag{11}$$

For incompressible flow, $(\partial U_k / \partial x_k)$ is small and the second term on the right side of equation (11) does not contribute significantly to the production. For compressible flow, $(\partial U_k / \partial x_k)$ is only large in regions with high velocity divergence, such as at shocks [12].

6. Mathematical description of RNG k-ε turbulent model in ANSYS CFX

The RNG k-ε model is based on renormalization group analysis of the Navier-Stokes equations. The transport equations for turbulence generation and dissipation are the same as those for the standard k-ε model, but the model constants differ, and the constant $C_{\varepsilon 1}$ is replaced by the function $C_{\varepsilon 1\mathrm{RNG}}$. The transport equation for turbulence dissipation becomes:

$$\frac{\partial(\rho \varepsilon)}{\partial t} + \frac{\partial}{\partial x_j}(\rho U_j \varepsilon) = \&\frac{\partial}{\partial x_j}\left[\left(\mu + \frac{\mu_t}{\sigma_{\varepsilon RNG}}\right)\frac{\partial \varepsilon}{\partial x_j}\right] + \frac{\varepsilon}{k}(C_{\varepsilon 1 RNG} P_k - C_{\varepsilon 2 RNG}\rho\varepsilon + C_{\varepsilon 1 RNG} P_{\varepsilon b}), \tag{12}$$

where

$$C_{\varepsilon 1\mathrm{RNG}} = 1.42 - f_\eta, \tag{13}$$

and

$$f_\eta = \frac{\eta\left(1 - \frac{\eta}{4.38}\right)}{(1 + \beta_{\mathrm{RNG}}\eta^3)}, \qquad \eta = \sqrt{\frac{P_k}{\rho C_{\mu RNG}\epsilon}}. \tag{14}$$

7. Mathematical description of the baseline k-ω model of turbulent

The Wilcox k-ω turbulence model is recognized for its sensitivity to freestream conditions, resulting in considerable fluctuations in simulation results based on the inlet ω value specified by Menter [16]. This sensitivity is regarded as a significant limitation, as it diminishes the model's robustness across diverse applications. Menter [16] proposed a hybrid approach that integrates the advantages of the k-ω model in proximity to the wall with the k-ε model in the external flow regions [12]. The methodology entails converting the k-ε model into a k-ω formulation and integrating both models into the simulation through a blending function, F_1. In this hybrid model, the Wilcox k-ω component is weighted by F_1, whereas the transformed k-ε model is weighted by $(1 - F_1)$. The blending function F_1 approaches one near the surface and progressively diminishes to zero with increasing distance from the wall. Thus, beyond the boundary layer, the conventional k-ε model is reinstated, guaranteeing more uniform and coherent outcomes throughout the boundary layer and freestream areas [12].

The Wilcox model will be as follows:

$$\frac{\partial(\rho k)}{\partial t}+\frac{\partial}{\partial x_j}\left(\rho U_j k\right)=\frac{\partial}{\partial x_j}\left[\left(\mu+\frac{\mu_t}{\sigma_{k1}}\right)\frac{\partial k}{\partial x_j}\right]+P_k-\beta'\rho k\omega, \tag{15}$$

$$\frac{\partial(\rho\omega)}{\partial t}+\frac{\partial}{\partial x_j}\left(\rho U_j \omega\right)=\frac{\partial}{\partial x_j}\left[\left(\mu+\frac{\mu_t}{\sigma_{\omega1}}\right)\frac{\partial \omega}{\partial x_j}\right]+\alpha_1\frac{\omega}{k}P_k-\beta_1\rho\omega^2. \tag{16}$$

Now the equations of the Wilcox model are multiplied by function F_1, the transformed k-ε equations by a function $(1 - F_1)$ and the corresponding k and ω equations are added to give the baseline (BSL) model. Including buoyancy effects, the BSL model is presented as follows [12]:

$$\frac{\partial(\rho k)}{\partial t}+\frac{\partial}{\partial x_j}\left(\rho U_j k\right)=\frac{\partial}{\partial x_j}\left[\left(\mu+\frac{\mu_t}{\sigma_{k3}}\right)\frac{\partial k}{\partial x_j}\right]+P_k-\beta'\rho k\omega+P_{kb}, \tag{17}$$

$$\frac{\partial(\rho\omega)}{\partial t}+\frac{\partial}{\partial x_j}\left(\rho U_j \omega\right)=\frac{\partial}{\partial x_j}\left[\left(\mu+\frac{\mu_t}{\sigma_{\omega3}}\right)\frac{\partial \omega}{\partial x_j}\right]+(1-F_1)2\rho\frac{1}{\sigma_{\omega z^2}\omega}\frac{\partial k}{\partial x_j}\frac{\partial \omega}{\partial x_j}+\alpha_3\frac{\omega}{k}P_k-\beta_3\rho\omega^2+P_{\omega b}\,. \tag{18}$$

The coefficients of the new model are a linear combination of the corresponding coefficients of the underlying models [12]:

$$\Phi_3=F_1\Phi_1+(1-F_1)\Phi_2. \tag{19}$$

The coefficients are equal to the following values: $\beta'=0.09,\ \alpha_1=5/9,\ \ \beta_1=0.075,\ \sigma_{k1}=2,\ \sigma_{\omega1}=2,$ $\alpha_2=0.44, \beta_2=0.0828, \sigma_{k2}=1, \sigma_{\omega2}=1/0.856.$

8. The mathematical description of Shear Stress Transport turbulence model

The k-ω based Shear Stress Transport (SST) model effectively accounts for the transport of turbulent shear stress, providing highly accurate predictions regarding the initiation and extent of flow separation under adverse pressure gradients [12].

The BSL model integrates the benefits of the Wilcox and k-ε models. However, it still inadequately predicts the initiation and extent of flow separation from smooth surfaces. This deficiency is discussed in detail by Menter [16], but primarily arises because these models, which do not account for the transport of the turbulent shear stress, overpredict the eddy viscosity. The appropriate transport behavior can be achieved through a limiter applied to the eddy-viscosity formulation:

$$v_t=\frac{a_1 k}{max(a_1\omega, SF_2)}. \tag{20}$$

The original formulation for the rest of the flow:

$$v_t=\mu_t/\rho. \tag{21}$$

F_2 is a blending function similar to F_1, which restricts the limiter to the wall boundary layer, as the underlying assumptions are not correct for free shear flows. S is an invariant measure of the strain rate. The production term of P_ω is given by [12]:

$$P_\omega=\left(\frac{\alpha_3}{v_t}\right)P_k. \tag{22}$$

It should be mentioned that this formulation differs from the standard k-ω model and in SST model $\sigma_{k1}=1.176$ [12].

9. The mathematical explanation of Eddy Dissipation Model of combustion simulation

As Li, Q et al. [17] described in their research the Eddy Dissipation Model (EDM) is based on three assumptions: 1 – the combustion reaction rate is infinitely fast; 2 – the fuel consumption rate in turbulent diffusion flames is solely determined by the turbulent mixing rate of fuel and oxidizer; and 3 – the fuel consumption rate is

inversely proportional to the turbulent time scale (k divided by ε). According to these assumptions, Magnussen and Hjertager [18] gave the following fuel reaction rate expressions:

$$f + S \cdot o = (1 + S)p, \tag{23}$$

$$R = \rho \frac{\varepsilon}{k} A \cdot min\left[Y_f, \frac{Y_o}{S}, B\frac{Y_p}{(1+S)}\right], \tag{24}$$

where f is fuel; o is oxidizer; p is combustion product; S is stoichiometric mass ratio of oxidizer to fuel; ρ is density; ε is turbulent dissipation rate; k is turbulent kinetic energy; Y is mass fraction of the corresponding species.

The parameters A=0.4 and B=0.5 are utilized in the combustion modeling framework. While just constant A is required for the simulation of diffusion flames, constant B is specifically made for simulating premixed flames [17].

The Eddy Dissipation Model (EDM) has been widely used in a range of CFD simulations, especially in gas turbine combustion studies [19], [20], and [21]. It has been incorporated into popular commercial CFD software programs, including Fluent, Star-CD, and ANSYS CFX. [17].

10. The mathematical explanation of Finite Rate Chemistry of combustion simulation

The Finite Rate Chemistry (FRC) model, as implemented in CFX, assumes that the rate of progress of elementary reaction k can be reversible only if a backward reaction is defined where [I] is the molar concentration of component I and F_k and B_k are the forward and backward rate constants respectively. Therefore, the rate of progress is computed as:

$$P_\omega = \left(\frac{\alpha_3}{v_t}\right) P_k. \tag{25}$$

The reaction order of component I in the elementary reaction k is presented by r. This reaction order is equal to the stoichiometric coefficient for elementary reactions, but it can be different for certain global reactions [12].

$$R_k = \left(F_k \prod_{I=A,B,\ldots}^{N_C} [I]^{r'_{kl}} - B_k \prod_{I=A,B,\ldots}^{N_C} [I]^{r''_{kl}}\right). \tag{26}$$

The only built-in formula for the forward and backward rate constants assumes an Arrhenius temperature dependence as:

$$F_k = A_k T^{\beta_k} \exp\left(-\frac{E_k}{RT}\right); \tag{27}$$

$$B_k = A_k T^{\beta_k} \exp\left(-\frac{E_k}{RT}\right), \tag{28}$$

where A_k is pre-expansional factor; β_k is dimensionless temperature exponent; E_k is the activation energy, T is the absolute temperature.

R_k can also be specified directly without using the relations. A_k, β_k and E_k are applied to forward and backward rates [12].

11. The combination of Eddy Dissipation Model and Finite Rate Chemistry

For the combined Eddy Dissipation Model and Finite Rate Chemistry (EDM/FRC), the reaction rates are first estimated for each model individually, and then the minimum of the two is employed. This approach is conducted for each reaction step separately, thus although the rate for one step may be restricted by the chemical kinetics, some other step might be limited by turbulent mixing at the same time and physical location. It is also feasible to apply distinct combustion models to each of the steps in a multi-step scheme. Some of the preconfigured schemes make advantage of this functionality, regardless of the global model selection. The combined model is suitable for a wide range of configurations, provided the flow is turbulent. In particular, the model is valid for numerous reactions that range from low to high Damköhler numbers (chemistry slow/fast compared to turbulent time scale). Use of this model is recommended if response rates are limited by turbulent mixing in one section of the domain and limited by kinetics somewhere else. The Eddy Dissipation model can, however, be more robust than Finite Rate Chemistry or the combination model [12].

12. The mathematical description flamelet model of combustion

Flamelet equations are a simplified form of the species and energy conservation equations, often used in combustion modeling to depict the interplay between turbulent flows and chemical reactions [23]. The theoretical underpinning and formulation of these flamelet equations are given by Peters [22] which can be represented as:

$$\rho \frac{\partial Y_i}{\partial t} - \frac{\rho \chi}{2} \frac{d^2 Y_i}{dZ^2} - \dot{\omega}_i = 0; \tag{29}$$

$$\rho \frac{\partial T}{\partial t} + \frac{\rho \chi}{2} \frac{d^2 T}{dZ^2} - \frac{1}{c_p} \sum_{i=1}^{N} h_i \dot{\omega}_i + \frac{Q_R}{c_p} = 0, \tag{30}$$

where Y_i is the mass fraction of species *i*; *T* is the temperature; $\dot{\omega}_i$ is the source term or the reaction rate of species *i*; Q_R is the radiative heat loss; h_i is enthalpy of species *i*; χ is the scalar dissipation rate, which quantifies the rate of mixing between fuel and oxidizer, and it represents the gradient of the mixture fraction perpendicular to the flame surface, which can be defined as [23]:

$$\chi = 2D \left(\frac{dZ}{dy}\right)^2, \tag{31}$$

where *D* is diffusion coefficient.

In ANSYS CFX an external program CFXRIF solves these equations to obtain a laminar flamelet table, which is integrated using beta PDF to have the turbulent flamelet library. This library provides the mean species mass fraction as functions of mean mixture fraction, variance of mixture fraction and turbulent scalar dissipation rate [12].

13. A brief explanation about the P-1 radiation model in ANSYS CFX

The P-1 radiation model in ANSYS CFX is a simple way for simulating radiative heat transfer in participating media, such as combustion gasses, where thermal radiation is relevant. Based on the spherical harmonics approximation of the radiative transfer equation, the P-1 model is computationally efficient compared to more complex methods like the discrete ordinates model (DOM). It simplifies radiation by considering it as a diffusion process, assuming that the radiative strength fluctuates continuously, making it suited for optically thick media where radiation dominates. The P-1 model allows for absorption, emission, and scattering of radiation and uses only the first term of the spherical harmonics expansion to solve the radiation transport. While it is less accurate in optically thin regions or in problems with sharp radiation gradients, the P-1 model provides a practical approach for capturing overall radiative effects in large-scale simulations, such as those in gas turbine combustion chambers, where it balances accuracy with computational efficiency [24].

14. The strategy of NO_x modeling in this simulation

Nitrogen oxides (NO_x) are mainly created by the reaction between the oxygen and nitrogen radicals in the flame at temperatures higher than 1800 K (1527 °C). Nitric oxide (NO), also referred to as Zeldovich NO, is created by a sequence of chemical events that were first described by Zeldovich in 1946 and then further developed by Baulch and associates in 1994 [25]. Two crucial processes (R1 and R2) in which nitrogen and oxygen radicals interact at high temperatures are involved in the Zeldovich mechanism. Third reaction (R3) can also play a major role in NO generation under some conditions, especially close to the stoichiometric air-fuel ratio.

Because of the large activation energy needed to break the strong bond in nitrogen (N_2) molecules and the rapidity of the reactions at high temperatures, this process is known as the "thermal" NO mechanism. The kinetics of each of the three reactions control their respective rates, with the first reaction acting as the rate-limiting step for the total production of thermal NO [25]. R is referring to the reaction.

$$O + N_2 \overset{k_1}{\rightarrow} NO + N \qquad \rightarrow \qquad k_1 = (1.8 \cdot 10^{11}) \exp\left(-\frac{38370}{T}\right); \tag{R1}$$

$$N + O_2 \overset{k_2}{\rightarrow} NO + O \qquad \rightarrow \qquad k_2 = (6.4 \cdot 10^{9}) \exp\left(-\frac{3162}{T}\right); \tag{R2}$$

$$N + O_2 \overset{k_3}{\rightarrow} NO + O \qquad \rightarrow \qquad k_3 = 3.0 \cdot 10^{3}. \tag{R3}$$

Referring to the reactions when multiply the rates of reaction, by the concentrations of the species involved in the reaction process and express it in [kmol/m³/s] it can then convert this outcome into a mass source term. This term indicates how much mass is being produced or used up, per unit volume within the system.

$$\frac{d[NO]}{dt} = k_1[O][N_2] + k_2[N][O_2] + k_3[N][OH]; \tag{32}$$

$$\frac{d[NO]}{dt} = k_1[O][N_2] - k_2[N][O_2] - k_3[N][OH]. \tag{33}$$

In ANSYS CFX Solver Theory Guide [12], the thermal formation in, $\mathrm{kg/m^3/s}, S_{NO,\,\mathrm{thermal}}$, as described, is therefore related to the rate of Reaction (R1):

$$S_{No,thermal} = 2W_{No}\,k_{thermal}[O][N_2]k_{thermal} = k_1. \tag{34}$$

This denotes the molecular mass of NO. Therefore, if the molar concentrations [O] and [N_2] of O radicals and N_2 are established, the thermal NO mechanism can be assessed [12].

In the other hand prompt, NO formation occurs when temperatures drop below 1800 K and since our simulation is conducted at temperatures exceeding 2000 K, we won't concentrate into the details of how NO forms but will incorporate the thermal formation of NO into the simulation. The detailed description can be found in [12]

In the process of organization of a CFD simulation we address the mass transport equation concerning the NO species by considering factors, like convection, diffusion, NO generation and consumption of species. This approach is essentially rooted in the concept of preserving mass. To accurately represent prompt reactions, we rely on the transport equation specific to the NO species [25]

$$\rho\frac{\partial Y_{NO}}{\partial t} + \rho u_i\frac{\partial Y_{NO}}{\partial x_i} = \frac{\partial}{\partial x_i}\left(\rho D\frac{\partial Y_{NO}}{\partial x_i}\right) + S_{NO}. \tag{35}$$

The source term S_{NO} is to be determined for different NO_x formation mechanism.

15. The geometrical parameters of the studied combustion chamber, boundary conditions and mesh

In this section, a tubular gas turbine combustion chamber modeled after the TAY combustor in a Rolls-Royce RB 183 turbofan engine (Fig.3) was utilized. The flame tube features six primary holes and twelve dilution holes. The swirler has 18 curved vanes positioned at a 45° angle, each with a thickness of 0.5 mm. The fuel injector includes 10 holes with a diameter of 1.7 mm, arranged on a cone at a 45° angle relative to the combustor's axis [26]. Some researchers, such as W.P. Jones et al. [27],[28], Heitor, M. et al. [29], Mohammadpour, M. et al. [30], Wang, J. Et al. [31] have also used this type of combustor in their investigations.

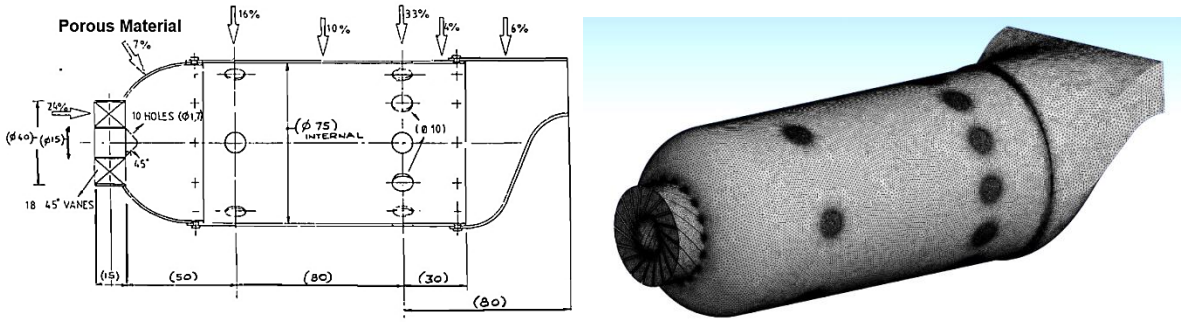

a *b*

Fig.3. The primary geometrical parameters of TAY combustor with the percentage of air distribution entering the liner [27] (*a*) and 3D schematic of combustion chamber with computational unstructured mesh (*b*).

The combustor is fabricated from a laminated porous sheet material, known as "Transply" and consists of a hemispherical head followed by a circular barrel of 74 mm diameter [27].

The boundary conditions were based on the experimental work of W.P. Jones et al. [27]. The conditions specified were as follows: the temperature of the air entering the combustion chamber was 523K, with a mass flow rate of 0.085 kg/s, while the fuel (C3H8-propane) had a mass flow rate of 1.65 g/s. The pressure within the combustion chamber was maintained at atmospheric levels. The air distribution was detailed, with 24% entering through the axial swirler, 16% through the primary cooling holes, and 33% through the secondary or dilution holes. Additionally, 27% of the air entered through a porous sheet metal. Due to insufficient information on the material characteristics of this porous sheet metal, along with the complexity of its geometric parameters, it was not modeled in our simulation. The simulations employed unstructured grids to accommodate the complex swirl geometry and the injector holes with about 5000 000 elements which is shown in Fig.3,*b*. This approach ensured a more accurate representation of the physical phenomena within the combustion chamber.

16. Results and discussion for validation of outlet temperature distribution and NO formation

The CFD simulation results of this research are shown in Fig.4,*a* for outlet temperature distribution and in Fig.4,*b*. for outlet NO distribution in various combustion and turbulence models.

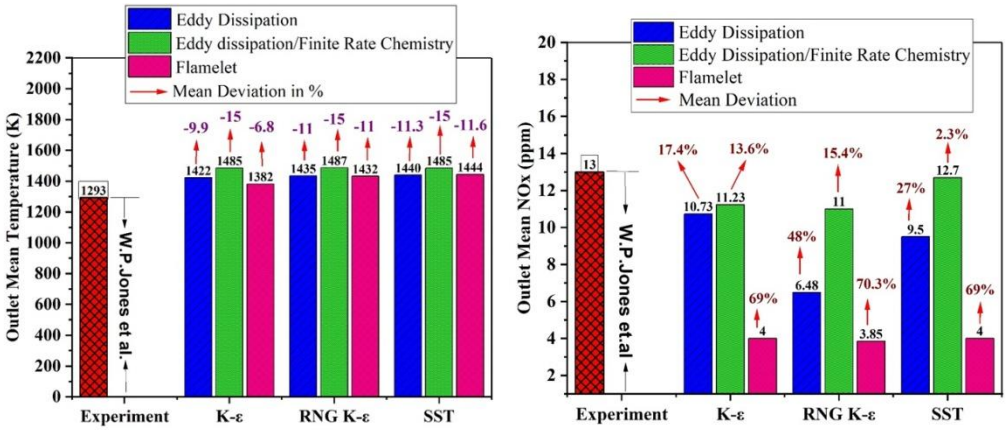

a *b*

Fig.4. Simulation results for outlet temperature distribution (*a*) and for outlet NO distribution in various combustion and turbulence models (*b*).

Here, we talk about the CFD results for the temperature at the combustor exit and contrast them with the findings of W.P. Jones et al.'s experiment [27]. It was stated that the combustor outlet's experimental mean temperature was 1293 K. To evaluate the accuracy of the anticipated temperatures and their differences from the observed value, we ran CFD simulations with a variety of turbulence and combustion models. A mean temperature of 1422 K was obtained from the simulations utilizing the k-ε turbulence model with the eddy dissipation model. This represents a mean deviation of -9.9% from the observed measurement. The mean temperature rose to 1485 K when the k-ε model was coupled with the finite rate chemistry and eddy dissipation model, leading to a greater variation of -15%. When the flamelet and k-ε models were combined, the mean temperature was 1382 K with a -6.8% deviation. Similarly, a mean temperature of 1435 K was obtained from simulations utilizing the eddy dissipation model and the RNG k-ε turbulence model, which differed by -11% from the actual finding. A mean temperature of 1487 K was likewise obtained by combining the RNG k-ε model with the finite rate chemistry and eddy dissipation models, which matched the deviation of -15%. The RNG k-ε model with the flamelet model yielded an 11% mean deviation and a mean temperature of 1432 K. The eddy dissipation model projected a mean temperature of 1414 K with a mean deviation of -11.3% for the SST turbulence model. The mean temperature was 1485 K with a -15% deviation when the SST model was integrated with the eddy dissipation and finite rate chemistry models. With a deviation of -11.6%, the mean temperature calculated using the SST model in conjunction with the flamelet model was 1444 K. As compared to the experimental result of 1293 K, the CFD findings show varied degrees of accuracy in combustor output temperature prediction. The flamelet model often exhibits the fewest discrepancies across all turbulence models across the many models studied. In particular, the combination of the flamelet and k-ε models yields the best agreement with the

experimental data, with a mean deviation of just -6.8%. This indicates that the flamelet model best describes the thermal behavior at the combustor outlet in this set of simulations when combined with the k-ε turbulence model.

With mean deviations ranging from -9.9% to -15%, the eddy dissipation and combination models overpredict the temperature more than other models, although offering insights. The flamelet model is the most accurate method for predicting the combustor outlet temperature in this study since it shows a more precise forecast, especially when used in conjunction with the k-ε turbulence model. This strong agreement with actual data demonstrates how well the flamelet model captures the intricate interactions that occur during combustion, leading to more accurate temperature estimates at the combustor outlet.

Here, we examine the CFD findings for NO concentration, which are presented in Fig.4,*b*, in parts per million (ppm) at the combustor output, and compare them with the experimental data reported by W.P. Jones et al. [27]. The experimental mean NO concentration at the combustor exit was reported to be 13 ppm. We conducted CFD simulations using several turbulence and combustion models to examine the accuracy of the projected NO concentrations and their deviations from the observed value.

The simulations utilizing the k-ε turbulence model with the eddy dissipation model resulted in a mean NO concentration of 10.73 ppm, which equates to a mean deviation of 17.4% from the observed value. When the k-ε model was integrated with the eddy dissipation model and finite rate chemistry, the mean NO concentration increased to 11.23 ppm, resulting in a reduced deviation of 13.6%. However, the k-ε model combined with the flamelet model gave a mean NO concentration of just 4 ppm, suggesting a huge divergence of 69%.

Similarly, simulations utilizing the RNG k-ε turbulence model with the eddy dissipation model gave a mean NO concentration of 6.48 ppm, deviating by 48% from the actual finding. The coupling of the RNG k-ε model with the eddy dissipation and finite rate chemistry model resulted in a mean NO concentration of 11 ppm, with a deviation of 15.4%. The RNG k-ε model with the flamelet model gave a mean NO concentration of 3.85 ppm, resulting in an even higher mean deviation of 70.3%.

For the SST turbulence model, the eddy dissipation model projected a mean NO concentration of 9.5 ppm, with a mean deviation of 27%. When the SST model was integrated with the eddy dissipation and finite rate chemistry model, the mean NO concentration was 12.7 ppm, resulting in the least deviation of 2.3%. The SST model combined with the flamelet model yielded a mean NO concentration of 4 ppm, with a mean deviation of 69%.

The CFD findings demonstrate varied degrees of accuracy in estimating the NO concentration at the combustor outlet compared to the experimental result of 13 ppm. Among the several models investigated, the combination of the SST turbulence model with the eddy dissipation and finite rate chemistry model demonstrates the highest agreement with the experimental data, with a mean NO concentration of 12.7 ppm and a deviation of just 2.3%. This shows that this combination most correctly mimics the NO generation and destruction mechanisms in the combustor. Other combinations, such as the k-ε with eddy dissipation and finite rate chemistry model and the RNG k-ε with eddy dissipation and finite rate chemistry model, also produce good forecasts with deviations of 13.6% and 15.4%, respectively. However, the flamelet model, regardless of the turbulence model utilized, consistently underpredicts the NO concentration, resulting in a substantial deviation of roughly 67-90%.

The SST turbulence model combined with the eddy dissipation and finite rate chemistry model is the most dependable strategy in this study for simulating NO concentrations at the combustor output. This strong agreement with experimental data underlines the efficiency of this model combination in effectively modeling the complicated chemical kinetics and turbulent mixing mechanisms that influence NO production in the combustion process.

It is crucial to note that the results of the CFD simulations may differ from the real experimental findings, owing to the absence of certain physical features of solid materials in the model. Specifically, the combustion liner in the experimental setup by W.P. Jones et al. [27], was constructed of a porous material, which was not predicted in our CFD models. The porous material of the combustion liner may greatly impact the combustion dynamics, including air flow, fuel-air mixing, and heat transmission. Porous materials can promote cooling and offer more consistent temperature distribution by enabling air to permeate through the liner, hence altering NO production rates. The exclusion of this porous property in our simulations likely leads to inconsistencies between the CFD findings and the experimental data. Consequently, while our models give significant insights and fair approximations, they might not fully represent the intricacies of the true combustion process seen in the experimental setting. Therefore, future studies might benefit from including the impacts of the porous liner to generate more realistic models that better match the experimental settings.

17. The contour plots of temperature distribution

The temperature distribution of C_3H_8 with air during combustion is shown in Fig.5,*a* in the combustion chamber. As we can see in Fig.5,*b*, the highest temperature forms in the center of the combustor and extends towards the combustor exit. The intensive combustion activity centered along the combustor's axis is indicated by this centrally located high-temperature area. Furthermore, the entry of cooling air through the primary and secondary cooling apertures into the combustion chamber is depicted in Fig.5,*a*. By combining with the hot combustion gases and lowering the ambient temperature close to the combustor walls, this cooling air helps to moderate the temperatures inside the combustor. The temperature profile shows how the heat produced during combustion is dispersed throughout the combustor, with the core experiencing the highest temperatures, which progressively drop toward the walls.

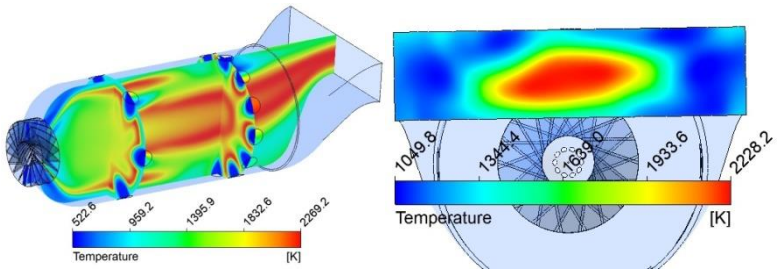

a *b*

Fig.5. Temperature distribution contours: at cross section and around primary and secondary cooling holes (*a*); at combustor outlet (*b*).

Comprehending the combustor's thermal behavior and how it affects material stress and NO_x formation, two critical variables for maximizing combustion efficiency and lowering emissions requires a comprehension of this distribution. The CFD model's correct depiction of this temperature distribution emphasizes how crucial it is to use the right turbulence and combustion models in order to fully portray the intricate interactions that occur during combustion.

18. The contour plots of NO formation

Fig.6,*a* depicts the NO formation along the combustion chamber in the cross section, showing the impact of primary and secondary cooling air on NO concentrations.

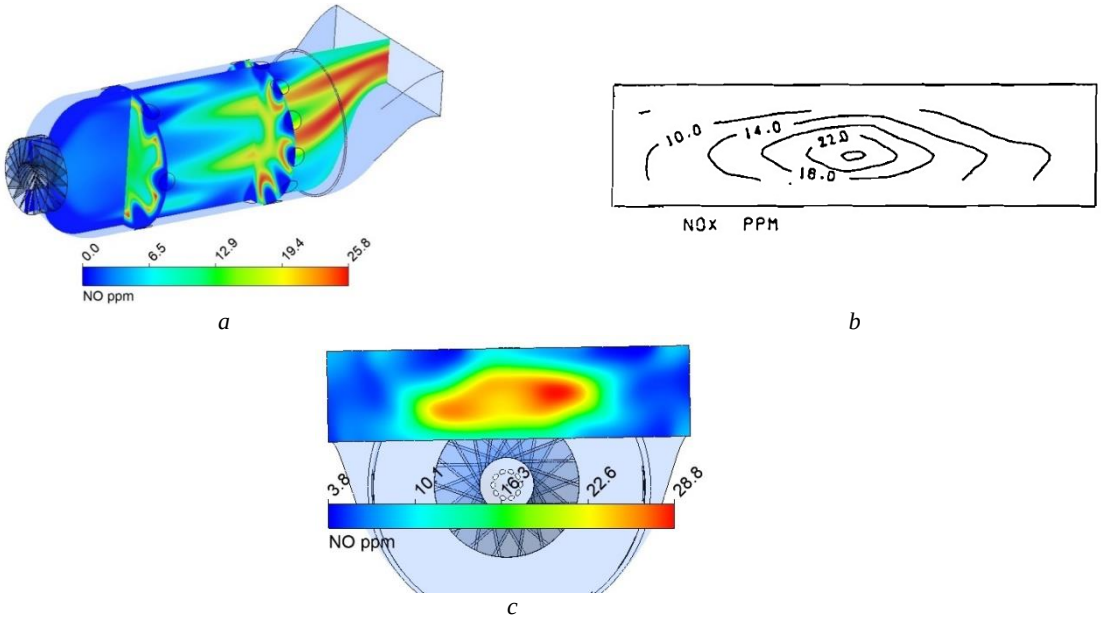

a *b*

c

Fig.6. NO concentration: along the cross section and around the primary and secondary cooling holes (*a*); experimental NO concentration contours made by W.P Jones et al. [27] (*b*); at the combustor outlet (*c*).

The injection of cooling air through the primary and secondary cooling holes affects the combustion process by moderating temperatures and modifying the local combustion chemistry, which in turn affects NO production.

This cooling air serves to minimize the peak temperatures in the combustion chamber, therefore reducing the NO generation mechanisms, principally driven by the high-temperature Zeldovich mechanism. The largest NO production occurs at the combustor exit and in the area immediately after the passage of cooling air through the dilution holes. This cooling air drives the flame to become thinner and extends it, which optimizes the circumstances for NO production near the outflow. In Fig.6,*b* the NO concentration contour is displayed as defined by W.P. Jones et al. [27] in their experimental research at the combustor outlet. The experimental NO concentration contours offer a precise picture of NO distribution, illustrating the combined impacts of combustion dynamics and cooling air interactions. Our CFD simulation findings, which are presented in Fig.6,*c*, demonstrate a significant agreement with these data contours, demonstrating that our model accurately represents the essential processes regulating NO generation and distribution at the exit plane of the combustor. This agreement between the CFD results and the experimental data validates the reliability and accuracy of our simulations in predicting NO concentrations, affirming the effectiveness of the chosen turbulence and combustion models in representing the complex interactions within the combustion chamber. The location of maximum NO generation at the combustor outlet, as demonstrated in both the experimental and CFD data, highlights the major impact of cooling air penetration and flame structure in influencing NO emissions.

19. The mesh sensitivity analysis

In this part of research, we examine the mesh sensitivity analysis on NO production at the combustor outlet using the k-ε turbulence model and the eddy dissipation combustion model. The analysis analyzes how different mesh resolutions affect the accuracy of NO concentration forecasts displayed in Fig.7. Three different mesh resolutions were used: a fine mesh with 10,011,554 elements, a moderate mesh with 3,438,212 elements, and a coarse mesh with 1,799,191 elements shown in Fig.7,*a*,*b*,*c*.

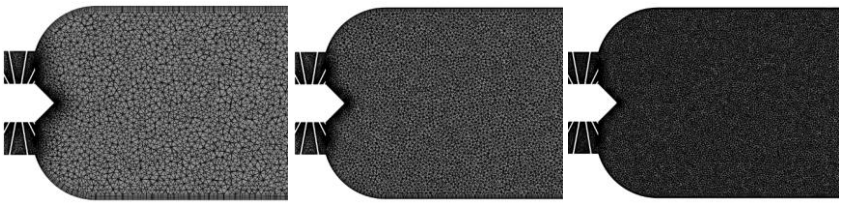

a *b* *c*

Fig.7. Various numbers of mesh elements: coarse (*a*); middle (*b*); fine (*c*).

The results in Fig.8 show that the fine mesh yields a NO concentration of 12 ppm at the combustor outlet, which corresponds to a mean deviation of 7.7% from the experimental data obtained by W.P. Jones et al., who reported a NO concentration of 13 ppm. This indicates that the fine mesh provides the highest accuracy among the meshes tested, closely approximating the experimental value.

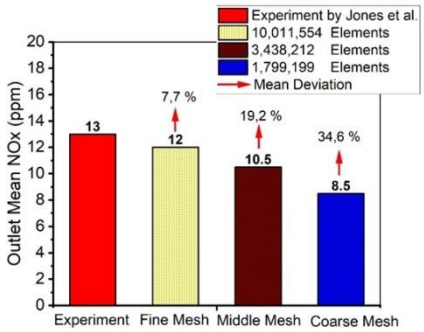

Fig.8. NO concentration at the combustor outlet at various numbers of mesh elements.

The middle mesh, with 3,438,212 elements, results in a NO concentration of 10.5 ppm at the outlet, leading to a mean deviation of 19.2% from the experimental data. While this mesh resolution still provides a reasonable prediction, the deviation is significantly higher than that of the fine mesh, indicating a lower accuracy. The coarse mesh, with 1,799,191 elements, predicts a NO concentration of 8.5 ppm at the outlet, which corresponds to a mean deviation of 34.6% from the experimental value. This large deviation indicates that the coarse mesh fails to capture the detailed flow and combustion characteristics necessary for accurate NO prediction.

The mesh sensitivity analysis highlights the importance of mesh resolution in accurately predicting NO concentrations in CFD simulations at the combustor outlet. The fine mesh, with its high resolution, captures the detailed turbulent mixing and chemical reactions more effectively, resulting in predictions that closely match the experimental data. In contrast, the middle and coarse meshes, with their lower resolutions, fail to adequately capture these complexities and flow behavior, leading to higher deviations from the experimental results. Therefore, the fine mesh is the best choice for accurately simulating NO formation at the combustor outlet, demonstrating good agreement with the experimental data. This analysis underscores the necessity of using sufficiently fine meshes in CFD studies to ensure reliable and accurate predictions, especially for phenomena involving complex interactions such as turbulent combustion and NO formation.

20. Conclusion

This experiment highlighted the usefulness of using RANS simulation of various turbulence and combustion models in accurately predicting temperature distribution and nitrogen oxide (NO_x) emissions at the output of the TAY combustion chamber of a Rolls-Royce RB 183 turbofan engine. The analysis demonstrated the great performance of the Flamelet model of combustion modeling paired with the k-ε turbulence model in predicting combustor outlet temperature with a minimal mean variation of -6.8%. For NO_x emissions prediction, the Shear Stress Transport turbulence model combined with the Eddy Dissipation and Finite Rate Chemistry models showed the highest accuracy, with a mean deviation of just 2.3% compared to experimental data analyzed by W.P. Jones. Besides that, as obvious from the obtained findings, the rest of the turbulence and combustion model combination has its own correctness. Mesh sensitivity analysis, which was performed with the help of unstructured meshes, emphasized the significance of fine mesh resolution in capturing intricate flow and combustion details, resulting in predictions closely aligned with experimental data, especially for NO_x concentrations at the combustor outlet. The fine mesh with over 10 million elements offered the most accurate findings, exhibiting a 7.7% variation from experimental NO_x measurements at the outflow, which was examined and introduced by W.P. Jones. The findings underscore the crucial relevance of optimal combustion and turbulence model selection and mesh resolution in establishing credible CFD simulations for combustion processes, delivering useful insights for upgrading gas turbine combustor designs and decreasing emissions.

References

[1] Oberkampf, W. L., & Trucano, T. G. (2002). *Verification and validation in computational fluid dynamics. Progress in Aerospace Sciences/Progress in Aerospace Sciences*, 38(3), 209–272. https://doi.org/10.1016/S0376-0421(02)00005-2

[2] Schlesinger, S. (1979) *Terminology for Model Credibility*. *Simulation*, 32, 103-104. https://doi.org/10.1177/003754977903200304

[3] Zhukov, V. P. (2012). Verification, Validation, and Testing of Kinetic Mechanisms of Hydrogen Combustion in Fluid-Dynamic Computations. *ISRN Mechanical Engineering*, *2012*, 1–11. https://doi.org/10.5402/2012/475607

[4] Bhurat, S., Pandey, S., Chintala, V., Jaiswal, M., & Kurien, C. (2022). Effect of novel fuel vaporiser technology on engine characteristics of partially premixed charge compression ignition (PCCI) engine with toroidal combustion chamber. *Fuel*, *315*, 123197. https://doi.org/10.1016/j.fuel.2022.123197

[5] Becker, L. G., Kosaka, H., Böhm, B., Doost, S., Knappstein, R., Habermehl, M., Kneer, R., Janicka, J., & Dreizler, A. (2017b). Experimental investigation of flame stabilization inside the quarl of an oxyfuel swirl burner. *Fuel*, *201*, 124–135. https://doi.org/10.1016/j.fuel.2016.09.002

[6] Aerospace Mechanical and Mechatronic Engineering - The University of Sydney. (n.d.). https://web.aeromech.usyd.edu.au/thermofluids/swirl.php

[7] Ferziger, J. H., & Perić, M. (2002). Introduction to Numerical Methods. In *Springer eBooks* (pp. 21–37). https://doi.org/10.1007/978-3-642-56026-2_2

[8] Eckbreth, A. C. (2022). *Laser Diagnostics for Combustion Temperature and Species*. https://doi.org/10.1201/9781003077251

[9] KoHse-HoingHaus, N. (2002). Applied Combustion Diagnostics. In *CRC Press eBooks*. https://doi.org/10.1201/9781498719414

[10] Masri, A. R. (2011). Design of Experiments for Gaining Insights and Validating Modeling of Turbulent Combustion. In *Fluid mechanics and its applications* (pp. 355–380). https://doi.org/10.1007/978-94-007-0412-1_15

[11] Borghi, R. (1988). Turbulent combustion modelling. *Progress in Energy and Combustion Science*, *14*(4), 245–292. https://doi.org/10.1016/0360-1285(88)90015-9

[12] ANSYS, Inc. (2015) ANSYS CFX-Solver Theory Guide, Release 16.2 https://www.ansys.com/

[13] Serbin, S., Burunsuz, K., Chen, D., & Kowalski, J. (2022). Investigation of the Characteristics of a Low-Emission Gas Turbine Combustion Chamber Operating on a Mixture of Natural Gas and Hydrogen. *Polish Maritime Research*, *29*(2), 64–76. https://doi.org/10.2478/pomr-2022-0018

[14] Launder, B. E., & Spalding, D. B. (1972). *Lectures in mathematical models of turbulence*. http://ci.nii.ac.jp/ncid/BA04677540

[15] Matveev, I. B., Serbin, S. I., Vilkul, V. V., & Goncharova, N. A. (2015). Synthesis Gas Afterburner Based on an Injector Type Plasma-Assisted Combustion System. *IEEE Transactions on Plasma Science*, *43*(12), 3974–3978. https://doi.org/10.1109/TPS.2015.2475125

[16] Menter, F. R. (1994). Two-equation eddy-viscosity turbulence models for engineering applications. *AIAA Journal*, *32*(8), 1598–1605. https://doi.org/10.2514/3.12149

[17] Li, Q., Yang, H., Wang, Y., & Wang, P. (2015). Accuracy improvement of the modified EDM model for non-premixed turbulent combustion in gas turbine. *Case Studies in Thermal Engineering*, *6*, 69–76. https://doi.org/10.1016/j.csite.2015.07.002

[18] Magnussen, B. F., & Hjertager, B. H. (1977b). On mathematical modeling of turbulent combustion with special emphasis on soot formation and combustion. *Symposium (International) on Combustion*, *16*(1), 719–729. https://doi.org/10.1016/S0082-0784(77)80366-4

[19] Gabler, H., Yetter, R., & Glassman, I. (1998). Asymmetric whirl combustion - A new approach for non-premixed low NO(x) gas turbine combustor design. *34th AIAA/ASME/SAE/ASEE Joint Propulsion Conference and Exhibit*. https://doi.org/10.2514/6.1998-3530

[20] Mongia, H. (2008). Recent Progress in Comprehensive Modeling of Gas Turbine Combustion. *46th AIAA Aerospace Sciences Meeting and Exhibit*. https://doi.org/10.2514/6.2008-1445

[21] Gobbato, P., Masi, M., Toffolo, A., & Lazzaretto, A. (2011). Numerical simulation of a hydrogen fuelled gas turbine combustor. *International Journal of Hydrogen Energy*, *36*(13), 7993–8002. https://doi.org/10.1016/j.ijhydene.2011.01.045

[22] Peters, N. (1984). Laminar diffusion flamelet models in non-premixed turbulent combustion. *Progress in Energy and Combustion Science*, *10*(3), 319–339. https://doi.org/10.1016/0360-1285(84)90114-x

[23] Chitgarha, F., & Mardani, A. (2018). Assessment of steady and unsteady flamelet models for MILD combustion modeling. *International Journal of Hydrogen Energy*, *43*(32), 15551–15563. https://doi.org/10.1016/j.ijhydene.2018.06.071

[24] Gamil, A. A., Nikolaidis, T., Lelaj, I., & Laskaridis, P. (2020). Assessment of numerical radiation models on the heat transfer of an aero-engine combustion chamber. *Case Studies in Thermal Engineering*, *22*, 100772. https://doi.org/10.1016/j.csite.2020.100772

[25] Jiang, B., Liang, H., Huang, G., & Li, X. (2006). Study on NOx Formation in CH4/Air Jet Combustion. *Chinese Journal of Chemical Engineering*, *14*(6), 723–728. https://doi.org/10.1016/S1004-9541(07)60002-0

[26] Gamil, A. A., Nikolaidis, T., Lelaj, I., & Laskaridis, P. (2020). Assessment of numerical radiation models on the heat transfer of an aero-engine combustion chamber. *Case Studies in Thermal Engineering*, *22*, 100772. https://doi.org/10.1016/j.csite.2020.100772

[27] Jones, W. P., & Toral, H. (1983). Temperature and Composition Measurements in a Research Gas Turbine Combustion Chamber. *Combustion Science and Technology*, *31*(5–6), 249–275. https://doi.org/10.1080/00102208308923645

[28] Bicen, A. F., & Jones, W. P. (1986). Velocity Characteristics of Isothermal and Combusting Flows in a Model Combustor. *Combustion Science and Technology*, *49*(1–2), 1–15. https://doi.org/10.1080/00102208608923900

[29] Heitor, M., & Whitelaw, J. (1986). Velocity, temperature, and species characteristics of the flow in a gas-turbine combustor. *Combustion and Flame*, *64*(1), 1–32. https://doi.org/10.1016/0010-2180(86)90095-7

[30] Mohammadpour, M., Houshfar, E., & Ashjaee, M. (2023). Combustion behavior study and flame zone analysis of biogas-fueled gas turbine combustor under O2/CO2 and O2/H2O oxidizing modes. *Fuel*, *345*, 128173. https://doi.org/10.1016/j.fuel.2023.128173

[31] Wang, J., Hu, Z., Du, C., Tian, L., & Baleta, J. (2021). Numerical study of effusion cooling of a gas turbine combustor liner. *Fuel*, *294*, 120578. https://doi.org/10.1016/j.fuel.2021.120578

Високоточне RANS CFD моделювання фізико-хімічних процесів горіння в камерах згоряння газових турбін в ANSYS CFX

Масуд Хаджіванд

Національний аерокосмічний університет ім. М. Є. Жуковського «Харківський авіаційний інститут», вул. Вадима Манька, 17, м. Харків, 61070, Україна

Анотація

У цьому дослідженні розглядається валідація і точність основних параметрів, включаючи розподіл температури і викиди оксидів азоту (NO_x) на виході з камери згоряння газової турбіни за допомогою високоточного CFD моделювання методом Нав'є-Стокса, усередненого за Рейнольдсом (RANS). Процес згоряння пропану(C_3H_8)-повітря моделюється в ANSYS CFX з використанням трьох різних моделей турбулентності, включаючи стандартну k-ε, RNG k-ε і перенесення напруги зсуву (SST), а також різних моделей горіння, таких як модель вихрового розсіювання (EDM), гібрид вихрового розсіювання і хімії кінцевих швидкостей (EDM/FRC), і модель полум'я, включаючи модель випромінювання P-1. Було проведено ретельний аналіз чутливості з використанням дрібних, середніх і грубих неструктурованих розрахункових сіток для підвищення надійності і точності результатів. Отримані результати моделювання показали, що для температури на виході стандартна модель турбулентності k-ε в поєднанні з моделлю горіння Flamelet дає середнє відхилення -6,8%, тоді як k-ε в поєднанні з EDM дає середнє відхилення -9,9%. Найменше відхилення викидів NO_x на виході з камери згоряння (2,3%) було отримано при використанні моделі згоряння EDM/FRC в поєднанні з моделлю SST. В той час, як та ж модель згоряння в поєднанні зі стандартною k-ε та RNG k-ε моделями продемонструвала більше середнє відхилення 13,6% та 15,4%, відповідно, при прогнозуванні викидів NO_x.

Ключові слова: горіння; емісія; обчислювальна гідрогазодинаміка; турбулентність; модель Flamelet; валідація; вихрове розсіювання.